Earth Planet. Sci. Lett. 648 (2024) 119113

Contents lists available at ScienceDirect

Earth and Planetary Science Letters

journal homepage: www.elsevier.com/locate/epsl

Local sedimentary effects shaped key sulfur records after the Great Oxidation Event

Roger N. Bryant [a,b,*], Jordan P. Todes [b], Jocelyn A. Richardson [c], Tara C. Kalia [b], Anthony R. Prave [d], Aivo Lepland [e,f], Kalle Kirsimäe [f], Clara L. Blättler [b]

[a] Department of Earth, Atmospheric, and Planetary Sciences, Purdue University, West Lafayette, IN 47907, USA
[b] Department of the Geophysical Sciences, University of Chicago, Chicago, IL 60637, USA
[c] SLAC National Accelerator Laboratory, Stanford Synchrotron Radiation Lightsource, Menlo Park, CA 94025, USA
[d] School of Earth and Environmental Sciences, University of St Andrews, St Andrews KY16 9TS, Scotland , United Kingdom
[e] Geological Survey of Norway (NGU), 7491 Trondheim, Norway
[f] Department of Geology, University of Tartu, Ravila 14A, 50411 Tartu, Estonia

ARTICLE INFO

Edited by Huiming Bao.

Keywords:
Great oxidation event
Lomagundi-jatuli excursion
Sulfur isotopes
Calcium isotopes
Diagenesis
Carbonate-associated sulfate

ABSTRACT

Our understanding of Earth's surface oxidant budget following the Great Oxidation Event (GOE) relies heavily on interpretations of carbon ($\delta^{13}C$) and sulfur ($\delta^{34}S$) isotope ratios. Isotopic data have been used to argue that a rise in marine sulfate concentrations to >10 mM during the GOE was followed by a sulfate reservoir 'collapse'. However, carbonate $\delta^{34}S$ and $\delta^{13}C$ values often reflect conditions specific to depositional setting and diagenetic alteration. To assess the relative importance of global vs. local/diagenetic controls, we present $\delta^{34}S$, $\delta^{26}Mg$, $\delta^{44/40}Ca$, and trace-metal data coupled with existing $\delta^{13}C$ data from the ca. 2.1–2.0 Ga Tulomozero Formation and the overlying Zaonega Formation in the Onega Basin (Karelia, Russia). Over this transitional interval, $\delta^{34}S$ and Sr/(Ca+Mg) values increase whereas $\delta^{13}C$ and $\delta^{44/40}Ca$ values decrease. X-ray absorption spectroscopy shows that the dominant form of sulfur within the rocks concomitantly shifted from mineralized sulfate and carbonate-associated sulfate (CAS) to variable mixtures of sulfide, sulfonate, and CAS. Those changes are associated with a depositional shift from shallow-marine to deeper-marine slope settings. $\delta^{44/40}Ca$ and Sr/(Ca+Mg) data indicate that depositional environmental changes drove a shift from seawater- to sediment-buffered carbonate recrystallization. Consequently, we interpret $\delta^{34}S$ trends that closely match those reported by previous workers as reflecting changing local environmental and diagenetic conditions, a finding that renders equivocal the use of such trends to assess sulfur cycle changes following the GOE. Our work establishes a blueprint for how to obtain deeper insight into the evolution of Earth's surface oxidation from stable isotope records.

1. Introduction

A series of oxidation episodes of Earth's surface are thought to have enabled the evolution of multicellular life, foremost of which was the 'Great Oxidation Event' [GOE (Holland, 2002)]. Spanning much of the early Paleoproterozoic (~2.4–2.1 Ga), the GOE is identified geologically by the appearance of non-marine redbeds, the disappearance of detrital pyrites and uraninites from the sedimentary record, and the decline in banded iron formations (Cloud, 1973). More quantitative evidence for the GOE lies in changes in the sulfur ($\delta^{34}S$, $\Delta^{33}S$) and carbonate carbon ($\delta^{13}C$) isotopic compositions of marine sedimentary rocks (Farquhar et al., 2000; Farquhar and Wing, 2003; Karhu and Holland, 1996; Planavsky et al., 2012; Schidlowski et al., 1975). Our focus is on the Paleoproterozoic sulfur isotope record, particularly the $\delta^{34}S$ values of marine sedimentary rocks. Prior to the GOE, oxidized (sulfate) and reduced (sulfide) bulk sedimentary sulfur sinks had similar average $\delta^{34}S$ values, but these reservoirs diverged sharply and, for the most part, permanently after the GOE (Canfield and Farquhar, 2009; Fike et al., 2015; Halevy et al., 2023). Interpreted through a steady-state box modeling approach, this change implies a secular increase in the relative burial proportion of oxidized sulfur (Fike et al., 2015), consistent with a more oxidizing ocean-atmosphere system during the GOE. This view is supported by evidence from evaporites for abundant (≥10 mmol/kg) marine sulfate around 2.1 Ga (Blättler et al., 2018). In concert with these

* Corresponding author.
E-mail address: rnbryant@purdue.edu (R.N. Bryant).

https://doi.org/10.1016/j.epsl.2024.119113
Received 13 May 2024; Received in revised form 9 October 2024; Accepted 9 November 2024
Available online 16 November 2024

changes in the sulfur cycle, the carbon cycle experienced the largest and longest-lived positive C-isotope excursion in Earth history, termed the Lomagundi-Jatuli Excursion (LJE) (Karhu and Holland, 1996; Melezhik and Fallick, 1996; Schidlowski et al., 1975). A prominent early interpretation of the LJE was that mass burial of organic carbon led to production of O_2 equivalent to 10–22 times its present-day level (Bekker and Holland, 2012; Karhu and Holland, 1996; Schidlowski et al., 1975). However, other geochemical proxies support more muted oxygenation (Hardisty et al., 2017; Scott et al., 2014) and questions remain about the magnitude, duration, and permanence of the GOE (Uveges et al., 2023) and LJE (Hodgskiss et al., 2023; Prave et al., 2022).

The latest cause for uncertainty about the LJE was the recognition that trends in carbonate $\delta^{13}C$ values are facies dependent, which casts doubt on interpretations that global mechanisms drive those trends (Hodgskiss et al., 2023; Prave et al., 2022). A similar reevaluation is due for Paleoproterozoic carbonate-associated sulfate (CAS) $\delta^{34}S$ data (Fig. 1). Earlier studies mostly took CAS $\delta^{34}S$ values to be a faithful proxy for the $\delta^{34}S$ value of coeval seawater sulfate, as CAS in modern carbonates exhibits minimal $\delta^{34}S$ offset from modern seawater (Kampschulte and Strauss, 2004). The sensitivity of seawater sulfate $\delta^{34}S$ to biogeochemical perturbation is inversely proportional to the mass of the sulfate reservoir. Therefore, the rate of change of an accurate record of seawater sulfate $\delta^{34}S$ can be used to estimate an upper limit for seawater sulfate concentrations (Kurtz et al., 2003). Based on this logic, a rise in CAS $\delta^{34}S$ after 2150 Ma (Fig. 1) was interpreted to reflect a transition from higher to lower sulfate concentrations soon after the LJE (Planavsky et al., 2012). This interpretation is broadly consistent with those from I/(Ca+Mg) (Hardisty et al., 2017), U in shales (Partin et al., 2013), and pyrite $\delta^{34}S$ and sulfate evaporite abundance (Scott et al., 2014), indicating a fall in oxygenation post-LJE.

Several recent studies have demonstrated the depositional, diagenetic, and mineralogical conditions at which CAS $\delta^{34}S$ is most likely to record the sulfur isotopic composition of contemporaneous seawater sulfate (Barkan et al., 2020; Bryant et al., 2022; Murray et al., 2021; Present et al., 2019, 2015; Richardson et al., 2021, 2019a, 2019b). Arguably the most widespread diagenetic effect on CAS $\delta^{34}S$ is co-occurring carbonate recrystallization and microbial sulfate reduction (MSR) below the sediment-water interface, which can lead to overprinting of seawater sulfate $\delta^{34}S$ values by residual ^{34}S-enriched sulfate in pore waters (Bryant et al., 2022; Murray et al., 2021; Rennie and Turchyn, 2014). This process can produce differences in CAS $\delta^{34}S$ values between different carbonate fabrics/textures in individual rock samples (Bryant et al., 2022; Present et al., 2019, 2015) and between different sedimentary facies in near-contemporaneous strata (Murray et al., 2021; Present et al., 2019). In the absence of a robust secular record of seawater sulfate $\delta^{34}S$ values as a baseline for comparison, it can be difficult to assess the effect of MSR on individual CAS $\delta^{34}S$ values.

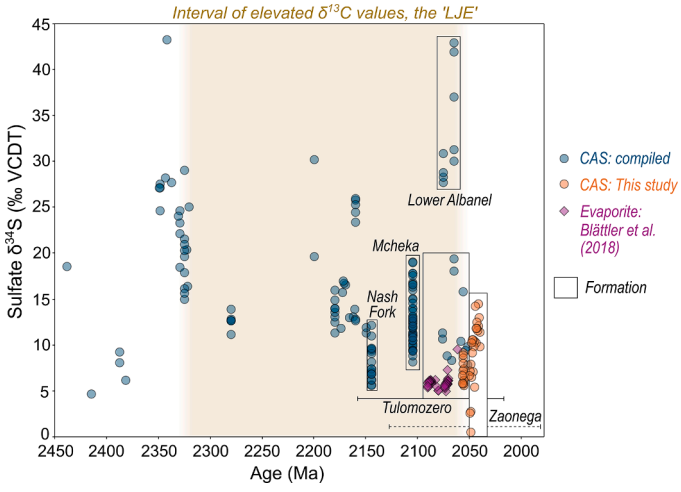

Fig. 1. Compilation of published CAS $\delta^{34}S$ values spanning the Lomagundi-Jatuli Excursion [after Planavsky et al. (2012) and Fike et al. (2015)], including those from this study, along with evaporite $\delta^{34}S$ data from the Tulomozero Formation as context (Blättler et al., 2018). Error bars shown are for the inferred ages of the Tulomozero Formation (solid) and Zaonega Formation (dashed). The approximate duration of the LJE is 2330–2060 Ma (Melezhik and Fallick, 1996).

A potential solution to this issue employs $\delta^{44/40}Ca$ and Sr/(Ca+Mg) measurements to identify CAS $\delta^{34}S$ overprinting by co-occurring MSR and carbonate recrystallization (Bryant et al., 2022; Lau and Hardisty, 2022). This approach relies on the sensitivity of carbonate $\delta^{44/40}Ca$ and Sr/(Ca+Mg) values to the evolving chemistry of pore fluids during early marine diagenesis. Here, we explain why $\delta^{44/40}Ca$ and Sr/(Ca+Mg) are effective indices for tracking different 'styles' of early marine diagenesis [see Ahm et al. (2018) for a more detailed consideration of this topic]. Firstly, primary carbonate minerals usually have $\delta^{44/40}Ca$ values that are considerably lower than that of the seawater in which they form (Higgins et al., 2018; Mills et al., 2021). When primary minerals dissolve in contact with pore fluids, the $\delta^{44/40}Ca$ of pore fluid progressively shifts from that of seawater to that of the primary mineral (Ahm et al., 2018; Higgins et al., 2018). As the fractionation (ε) between aqueous Ca and diagenetic carbonate is close to 0‰ (Fantle and DePaolo, 2007; Jacobson and Holmden, 2008), the $\delta^{44/40}Ca$ of diagenetic mineral tracks the extent of alteration of the pore water from which it precipitated. We describe the geochemistry of diagenetic minerals forming from unaltered seawater as 'seawater-buffered', and the geochemistry of diagenetic minerals forming from evolved pore waters as 'sediment-buffered'. For Sr/(Ca+Mg), primary carbonate minerals contain high Sr concentrations (particularly for aragonite), whereas diagenetic calcite and dolomite have much lower Sr concentrations due to their lower partition coefficients (Banner, 1995; Banner and Hanson, 1990). This diagenetic Sr decline is largest for carbonates forming in unaltered pore waters and slightly smaller for those forming in evolved fluids that have previously reacted with carbonate minerals, due to accumulation of Sr in the diagenetic fluid.

The depth profile of pore water sulfate $\delta^{34}S$ values evolves as a function of the balance between reaction (in this case MSR) and diffusive transport (often collectively referred to as 'system openness') (Bryant et al., 2023a; Claypool, 2004; Halevy et al., 2023; Jorgensen, 1979). Therefore, if there is spatiotemporal overlap between MSR and recrystallization, $\delta^{44/40}Ca$ and Sr/(Ca+Mg) values could be used to pinpoint samples with better-preserved (i.e., open-system) depositional CAS. Studies of modern pore waters suggest that MSR and recrystallization can operate on similar length scales (Bradbury and Turchyn, 2018; Teichert et al., 2009). MSR can also promote diagenetic carbonate precipitation by generating alkalinity (Gallagher et al., 2014), yielding, therefore, a mechanistic link between carbonate $\delta^{44/40}Ca$ and CAS $\delta^{34}S$ values. Furthermore, case studies of Pleistocene- and Permian-aged carbonate sediments display negative correlations between $\delta^{44/40}Ca$ and CAS $\delta^{34}S$ values (Bryant et al., 2022; Murray et al., 2021). Together, these studies suggest that coupled $\delta^{44/40}Ca$ and CAS $\delta^{34}S$ analyses have potential to clarify interpretations of CAS $\delta^{34}S$ records throughout Earth history.

Here, we present coupled $\delta^{44/40}Ca$, Sr/(Ca+Mg), $\delta^{26}Mg$ and CAS $\delta^{34}S$ data from the ~2.1 to 2.0 Ga upper Tulomozero Formation and lower Zaonega Formations in the Onega Paleobasin, northwestern Russia, that contain the LJE and its termination to test these ideas and reconstruct the marine sulfate reservoir post-GOE and through the LJE.

2. Materials and methods

The upper Tulomozero Formation consists of dolostone-dolomarl with evaporite fabrics, indicative of nearshore marine and sabkha settings (Brasier et al., 2011; Prave et al., 2022). The overlying Zaonega Formation consists of variably organic matter (OM)-rich mudstone (siliciclastic-dominated) and minor dolostone-dolomarl (locally termed

'krivozerite') deposited in open and deeper marine settings. It also records a decline from the strongly positive $\delta^{13}C$ values (up to +14‰) typifying the Tulomozero Formation to those centered around 0‰ (Prave et al., 2022). Although the depositional ages of the Tulomozero Formation [carbonate Pb-Pb age of 2090 ± 70 Ma (Ovchinnikova et al., 2007)] and the overlying Zaonega Formation [*Re*-Os age of ~2050 Ma (Hannah et al., 2008)] remain poorly constrained, the current age estimates overlap with those for the Nash Fork (USA), Lower Albanel (Canada), and Mcheka Formations (Zimbabwe) (Planavsky et al., 2012) (Fig. 1).

The evaporites of the lower Tulomozero Formation have been studied extensively, providing good context for sulfur cycle behavior during the LJE (Blättler et al., 2018), including from CAS (Reuschel et al., 2012). These studies show that the $\delta^{34}S$ value of seawater sulfate was mostly stable at ~5‰, with concentrations of ≥10 mmol/kg (Blättler et al., 2018). The sulfur cycle during deposition of the Zaonega Formation is less well constrained. The Zaonega Formation is mostly fine-grained siliciclastic rocks, hence unsuitable for conventional CAS studies using elemental analyzer isotope ratio mass spectrometry (EA-IRMS) (Paiste et al., 2022, 2020), but can be investigated using 'micro-CAS' methods which utilize multi-collector inductively coupled plasma mass spectrometry (MC-ICP-MS), and thus require three orders of magnitude less sulfur (Bryant et al., 2023b; Paris et al., 2013, 2014; Present et al., 2019). We apply the latter technique to characterize CAS $\delta^{34}S$ values from drill core samples recovered in the Onega Parametric Hole (OPH) (Krupenik and Sveshnikova, 2011) in the Onega Paleobasin in northwestern Russia, and to assess any change in the sulfate reservoir during this interval.

The base of the Zaonega Formation in the OPH core occurs at 2115 m and 40 powdered sedimentary rock samples were taken between depths of 1902 m to 2242 m. We targeted samples with clear primary (e.g., fine laminations or crossbedding) or early diagenetic (e.g., magnesite nodules) sedimentary textures, and avoided intervals containing obvious euhedral pyrite (see Fig. S1). $\delta^{13}C$ and $\delta^{18}O$ data have been previously published for the studied section (Prave et al., 2022), and data from equivalent stratigraphic heights and lithologies as samples used for this study are included in our figures.

2.1. Carbonate-associated sulfate extraction

Extraction and analysis for $\delta^{34}S$ of CAS was conducted using established methods (Bryant et al., 2023b; Paris et al., 2014, 2013; Present et al., 2019). Powdered samples (10–30 mg) were sequentially treated with 10% NaCl solution, 5% NaOCl, and methanol to remove soluble salts, organic-hosted sulfur compounds, and residual NaOCl, respectively. To assess the impact of the NaOCl (bleaching) step during CAS extraction on measured sulfate concentrations and $\delta^{34}S$ values, CAS $\delta^{34}S$ analyses were repeated for all samples without the NaOCl (bleaching) step. Unbleached samples generally had higher apparent CAS concentrations and substantially lower $\delta^{34}S$ values than their bleached counterparts (Fig. S2). This test shows that the bleaching step effectively removes organic sulfur, ensuring accurate CAS $\delta^{34}S$ determination.

After pre-treatments, samples were dissolved in 10–30 mL of a buffered acetic acid solution, which ensured complete carbonate dissolution without associated siliciclastic phases. A 5 mL aliquot of each sample was evaporated to dryness at 160 °C and run up in 800 μL 3.3 mN HCl. Samples were loaded onto 15 mL Biorad PolyPrep columns packed with 800 μL AG1-X8 anion exchange resin and allowed to equilibrate for 30 min. Cations were eluted from columns using 3 rounds of 800 μL ultrapure water and discarded. Anions were eluted from columns using 4 rounds of 800 μL 0.5 N HNO_3 and collected in Teflon vials. The anion fractions were evaporated to dryness and run up in 4 mL ultrapure water. A 500 μL aliquot was taken for anion quantification, as described below, and the remaining 3.5 mL were evaporated to dryness to be used for sulfur isotope analysis.

2.2. Automated ion chromatography (IC)

For sulfate, a sample aliquot was quantified in a Thermo/Dionex 6000 ion chromatography system using a NaOH eluent and a four-point concentration calibration. The remaining mass of sulfur in the Teflon vials was calculated, allowing all samples to be run up to ~50–100 ppb S in 2% HNO_3 for mass spectrometry.

For cations, dissolved sample aliquots were diluted with buffered acetic acid to yield solutions with Ca concentrations of 100–200 ppm or Mg concentrations of 10–15 ppm, as appropriate for the selected isotopic system. The selected element was collected via a Thermo/Dionex 6000 ion chromatography system using a methanesulfonic acid eluent; this method has the advantage of automation and quantification as compared to traditional manual column methods (Razionale et al., 2022). Once collected, samples were dried, treated with 16 N HNO_3 to oxidize and volatize column-derived organic compounds, dried again, and redissolved for isotopic analysis in 2% HNO_3.

2.3. Sulfur isotopes

Analyses were conducted on a Thermo Neptune XT MC-ICP-MS, coupled with an ESI Apex-Ω desolvating nebulizer, in the Blättler Laboratory at the University of Chicago. We used 200 ppb calcium as a dopant to maximize sulfur ionization efficiency and limit instrumental mass fractionation (IMF) variability (Bryant et al., 2023b), and diluted samples to account for evaporation during the run. To correct for IMF, all samples were bracketed by Ca-doped standard solutions, and all samples and brackets were further bracketed by pure Ca solution (machine blank). Each run involved 5 standards of known isotopic composition, 22 samples, and 3 procedural blanks. Procedural blank corrections for samples constituted subtracting the average abundances (adjusted by the relative dilution factor of sample compared to procedural blank) of ^{32}S, ^{33}S and ^{34}S for the procedural blanks measured in-run. Raw isotopic ratios are converted to ‰ Vienna Canyon Diablo Troilite (VCDT) (Ding et al., 1999) using the average seawater composition in each run, and the other standards are used to verify accuracy. The degree of mass independence is also assessed for each sample and standard; standards/samples with $\Delta^{33}S$ more than ±0.1‰ (close to the internal precision for this method) are discarded. Average long-term $\delta^{34}S$ measurements of IAEA-SO-5 and NBS-127 standards were 0.60 ±0.44‰ (2σ, $n = 25$) and 21.09±0.48‰ (2σ, $n = 22$), respectively – within error of published values. The long-term average value and external reproducibility (2σ, $n = 22$) in $\delta^{34}S$ for an in-house aragonite sand standard analyzed by this method is 22.29±0.60‰.

2.4. Calcium isotopes

Ca isotopic analyses were carried out using the instruments described in Section 2.3. To avoid further interferences, a medium-resolution slit was used to avoid major interferences (such as ArH_2^+) by maintaining a position on the low-mass shoulder. Sample-standard bracketing was used to correct for IMF. Sample and standard solutions were diluted to the same concentration to minimize concentration-dependent isotope effects, known linear concentration-dependent effects were corrected using a concentration calibration, and strontium interferences were corrected by monitoring the double-charged $^{87}Sr^{2+}$ beam. The ^{42}Ca, ^{43}Ca, and ^{44}Ca beams were measured: after correction, $\delta^{44/40}Ca$ values were calculated using established kinetic fractionation laws assuming no radiogenic ^{40}Ca excess (Young et al., 2002). The long-term external reproducibility of this calcium isotope measurement protocol is ±0.12‰ (2σ) (Bryant et al., 2022; Razionale et al., 2022). $\delta^{44/40}Ca$ values are reported with respect to IAPSO seawater (Wieser et al., 2004).

2.5. Magnesium isotopes

For magnesium isotope analyses, which were also conducted on the Neptune XT, samples were introduced using a dual-path glass cyclonic chamber using a low-resolution slit and corrected for instrumental mass bias via sample-standard bracketing (Bryant et al., 2022). The long-term external reproducibility of this magnesium isotope measurement protocol is ±0.10‰ (2σ). δ^{26}Mg values are reported with respect to the DSM3 reference standard (Galy et al., 2003).

2.6. X-Ray absorption near-edge spectroscopy (XANES)

Sulfur XANES spectra were collected on beamline 14–3 (imaging mode) at the Stanford Synchrotron Radiation Lightsource (SSRL), SLAC National Accelerator Laboratory, under standard ring conditions (500 mA and 3 GeV). Beamline 14–3 is equipped with a double-cooled Si 111 monochromator, which was calibrated to the S K-edge using the first pre-edge feature of a sodium thiosulfate powder (2472.02 eV). Although BL14–3 is principally a micro-focused imaging beamline, the focusing optic can be moved to use a larger beam. Slits were used to focus the beam to approximately 1 × 1 mm, for bulk XANES spectroscopy. Beamline 14–3 has a Hitachi Vortex 7-element Si drift detector which improves the signal to noise ratio in low S samples.

Samples were prepared as fine homogenous powders; a small amount of powder was placed onto S-free tape (Saint Gobain) and covered with 5 μm polypropylene thin film. Each sample packet was cut to approximately 5 × 5 mm in size and placed on top of a larger strip of S-free tape (polypropylene facing up) that was adhered to a sample holder, into an array of 3 × 3 samples per holder. This enabled minimal sample changes and increased efficiency of beamtime. Sample holders were loaded onto a multi-sample wheel which mounts onto a fully rotating 360° sample stage within a He-purged atmosphere (to reduce X-ray attenuation in air). Since bulk XANES spectroscopy was obtained in BL14–3 imaging mode, a camera video feed facilitated locating each sample within our 3 × 3 array on each holder. Two repeat XANES measurements were obtained per sample to improve signal-to-noise.

Data processing was performed using a combination of SIXpack (Webb, 2005) and Athena (Ravel and Newville, 2005). Repeat XANES spectra were inspected for diffraction in each detector channel, then averaged together in SIXpack. Subsequently, background subtraction and normalization were performed in Athena by fitting a linearized pre-edge and 2nd order polynomial to the post-edge. A linear combination fitting (LCF) was performed to identify the relative abundance of S species in the experimental XANES spectra. Based on the features observed in the experimental spectra, as well as anticipated S species in our samples, we supplied the following XANES references for LCF: pyrite (Manceau and Nagy, 2012), sulfonate (Manceau and Nagy, 2012), anhydrite (Anzures et al., 2020), and CAS (Richardson et al., 2019b). We chose sulfonate, rather than any reduced organic sulfur species, due to the limited variability of the energy position of the spectral feature at ~2481 eV (see, for example, Fig. S3). Due to the similar energy positions of features in sulfonate, sulfate ester and CAS, any feature at 2481 eV is attributed to either sulfonate or a sulfate ester and thus termed S-org to reflect the presence of an oxidized organic S moiety.

2.7. Trace element abundances

Sr/(Ca+Mg), and U/(Ca+Mg) were measured using a Thermo Scientific iCAP RQ inductively coupled plasma mass spectrometer (ICP-MS) in the Blättler Laboratory at the University of Chicago, following a previously described standard geochemical protocol (Bryant et al., 2022). In brief, small aliquots of the dissolved samples were subsampled, spiked with an internal standard solution, measured in STD mode, and quantified against a matrix-matched calibration curve.

2.8. Diagenetic model

We used an existing diagenetic model (Ahm et al., 2018), recently adapted to include MSR and CAS diagenesis (Bryant et al., 2022), to simulate the diagenesis of the Zaonega Formation carbonate component. Parameters used were identical to those in Bryant et al. (2022), unless stated otherwise here. Based on model-data fit (this study), primary carbonate mineralogy was assumed to be 10% low-Mg calcite and 90% aragonite, seawater $\delta^{44/40}$Ca was assumed to be −0.15‰, seawater δ^{26}Mg was assumed to be +0.4‰, seawater [Mg^{2+}] was assumed to be 30 mM, and diagenetic carbonate mineralogy was assumed to be 100% dolomite. Based on Blättler et al. (2018), we assumed a seawater sulfate δ^{34}S of 5‰, a seawater [Ca^{2+}] of 10 mM, and a seawater [SO_4^{2-}] of 10 mM; the latter two are likely minimum constraints. We explore the effects of relaxing assumptions about seawater [SO_4^{2-}] later. More complete sensitivity analyses of the model can be found in Ahm et al. (2018) and Bryant et al. (2022).

3. Results

3.1. Lithologies, carbonate mineralogy, Ca and Mg isotope ratios, and Sr/(Ca+Mg)

The upper Tulomozero Formation in the OPH core is characterized by moderate-to-high carbonate contents (20–100 wt%) whereas the Zaonega Formation is carbonate-poor (<20 wt%) excepting one interval (2025–1981 m depth) of carbonate-rich (avg. ~40 wt%) dolostone-dolomarl (krivozerite) strata. The carbonate mineralogy of the Tulomozero Formation is varied (Fig. 2) with Mg/(Ca+Mg) ratios ranging from ~0.15 (a mixture of low-Mg calcite and dolomite) to ~1 (magnesite), whereas the Zaonega Formation is mostly dolomitic.

$\delta^{44/40}$Ca values are quite variable in the Tulomozero Formation, with a median of −0.86‰, but are high in the lowermost Zaonega Formation (~−0.6‰) and decrease up-section to less than −1.0‰. In contrast, δ^{26}Mg values are relatively stable (median of −1.1‰), with a few samples having ^{26}Mg-enrichments that correspond to deviations from dolomite stoichiometry. Overall, the Mg isotopic composition is relatively heavy compared to typical Proterozoic and Phanerozoic dolomites (Bryant et al., 2022; Higgins et al., 2018; Riechelmann et al., 2020), particularly between 2000 and 1900 m depth, where the median value is −1.0‰.

Sr/(Ca+Mg) values are similar on average in the Tulomozero Formation (0.14×10^{-3} mol mol^{-1}) and the Zaonega Formation (0.13×10^{-3} mol mol^{-1}). Within the Zaonega Formation, Sr/(Ca+Mg) values generally increase up-section, averaging 0.12×10^{-3} and 0.16×10^{-3} mol mol^{-1} below and above 2000 m depth, respectively.

3.2. Sulfur speciation

In the Tulomozero Formation, XANES data for bulk powders indicate that sulfur is predominantly inorganic and oxidized (Fig. 2; Fig. S3) and present as variable mixtures of CAS and mineralized sulfate (e.g., $CaSO_4$). In the lower part of the Zaonega Formation (between 2115 and 2000 m), organic and inorganic species are present in both reduced and oxidized forms, with sulfur split between CAS, mineralized sulfide (e.g., pyrite), and organic sulfur (e.g., sulfonate). In the uppermost part of the Zaonega Formation, sulfonate is the dominant sulfur species, with minor CAS contributions.

3.3. Comparison between C, S, and Ca isotope geochemistry

The Tulomozero Formation features low and relatively invariant CAS δ^{34}S values (Fig. 2), with a median of 6.7‰. In the Zaonega Formation, CAS δ^{34}S values increase progressively up-section, mirroring the $\delta^{44/40}$Ca trend and following the Sr/(Ca+Mg) trend, with a median value of 11.8‰ above the krivozerite. Concentrations of CAS (calculated with

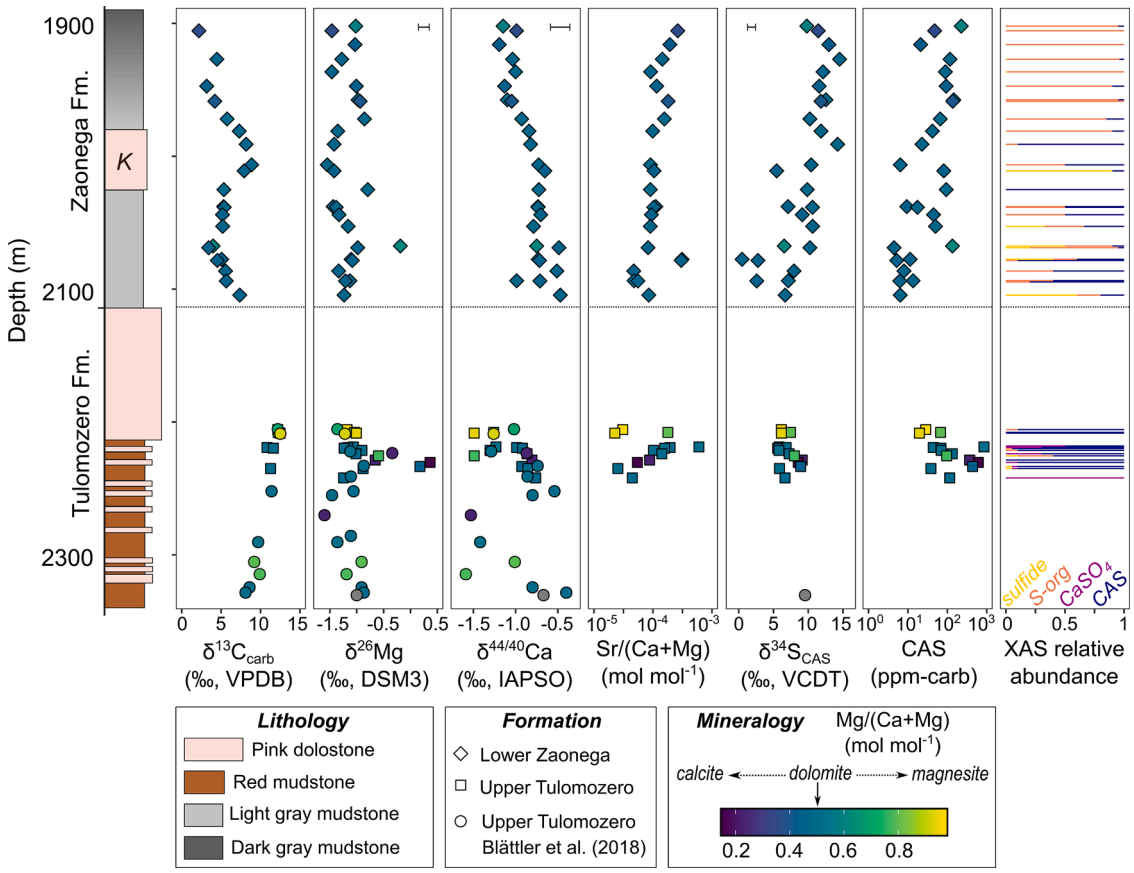

Fig. 2. Downcore geochemical trends of carbonate (acid-soluble) fraction in the upper Tulomozero and lower Zaonega formations in the OPH core. Simplified lithologic section and $\delta^{13}C$ data are after Prave et al. (2022) – 'mudstone' means siliciclastic-dominated fine-grained sediment. In the log, '*K*' stands for krivozerite. 'VPDB' is the Vienna Peedee belemnite reference standard (Coplen, 1995). Error bars shown at the top of $\delta^{26}Mg$, $\delta^{44/40}Ca$ and $\delta^{34}S$ panels are long-term external reproducibility (±2σ) for carbonate standards. Concentrations of CAS are listed in ppm for the carbonate fraction and error is ±10%. For other panels, errors are smaller than the symbols. No data are available for 2205–2117 m depths because no core was recovered from this interval. The relative abundance of S species was determined by linear combination fitting of bulk XAS data.

respect to the carbonate fraction) show no clear stratigraphic trends but are generally very low (median: 58 ppm; range: 4 to 850 ppm) and slightly lower in the Zaonega Formation (median: 43 ppm).

In the evaporite-bearing (magnesite- and anhydrite-dominated) lower Tulomozero Formation, $\delta^{34}S$ and $\delta^{13}C$ values obtained by Blättler et al. (2018) are mostly stable at ~5–6‰ and ~12‰, respectively (Fig. 3a, b), whereas $\delta^{44/40}Ca$ and $\delta^{26}Mg$ values are quite variable but higher on average than those reported here. Generally, both $\delta^{18}O$ and $\delta^{13}C$ values are higher in the Tulomozero Formation and decrease up-section into the Zaonega Formation, except for the $\delta^{13}C$ values in the krivozerite.

Comparisons between C, S, and Ca isotope data reveal several consistent patterns (Fig. 3). Data for the Tulomozero Formation define vectors of invariant $\delta^{34}S$ and $\delta^{13}C$ (Fig. 3a, c), and moderately variable $\delta^{44/40}Ca$ values (Blättler et al., 2018). Some outliers correspond to mineralogical variations, such as enrichments in Ca or Mg relative to normal dolomite stoichiometry implying mixing with calcite or magnesite.

Samples from the lower Zaonega Formation generally cluster in distinct parts of each phase space (Fig. 3b, d), including the lowest average $\delta^{13}C$ and higher, more variable CAS $\delta^{34}S$ values. Within the samples from the Zaonega Formation, moderate variations exist for all geochemical indices and define broad vectors of decreasing $\delta^{13}C$ and $\delta^{44/40}Ca$ and increasing CAS $\delta^{34}S$ values. $\delta^{44/40}Ca$ and CAS $\delta^{34}S$ are significantly negatively correlated (Fig. S4a; Pearson's correlation coefficient, $R = -0.52$; $p = 0.007$), with an improved correlation if the three anomalously low CAS $\delta^{34}S$ values are removed (Fig. S4b, $R = -0.57$; $p = 0.0043$).

4. Discussion

4.1. Deposition and diagenesis of the Tulomozero Formation

The evaporite-dominated lower Tulomozero Formation recovered in the OPH core was interpreted previously as evidence of high seawater sulfate concentrations (>10 mM) during the LJE and GOE (Blättler et al., 2018). Evaporite pseudomorphs and textures in the mixed carbonate-siliciclastic sediments in the upper Tulomozero Formation, including the presence of magnesite ($MgCO_3$) in some OPH samples (Melezhik et al., 2001), indicate that the depositional environment remained very shallow (Fig. 4b). All carbonates formed in this shallow marine setting have elevated $\delta^{13}C$ values, unlike those in contemporaneous deeper marine facies (Prave et al., 2022), suggesting that they initially formed in contact with locally ^{13}C-enriched DIC. Within the upper Tulomozero Formation, $\delta^{44/40}Ca$ variations partly reflect differences in sample mineralogy. For example, magnesite-dominated samples typically have lower $\delta^{44/40}Ca$ values than dolomite-dominated samples. Similarly, anomalous ^{26}Mg-enrichments occur in some calcite-rich samples, which could be related to secondary calcite precipitation [i.e., a product of dedolomitization (Črne et al., 2014)]. Given these mineralogical effects, we focus the remainder of our discussion on interpreting dolomite-dominated (>50%) samples, which constitute most samples in the upper Tulomozero Formation and all samples in the lower Zaonega Formation. We interpret the $\delta^{44/40}Ca$ (median −0.9‰),

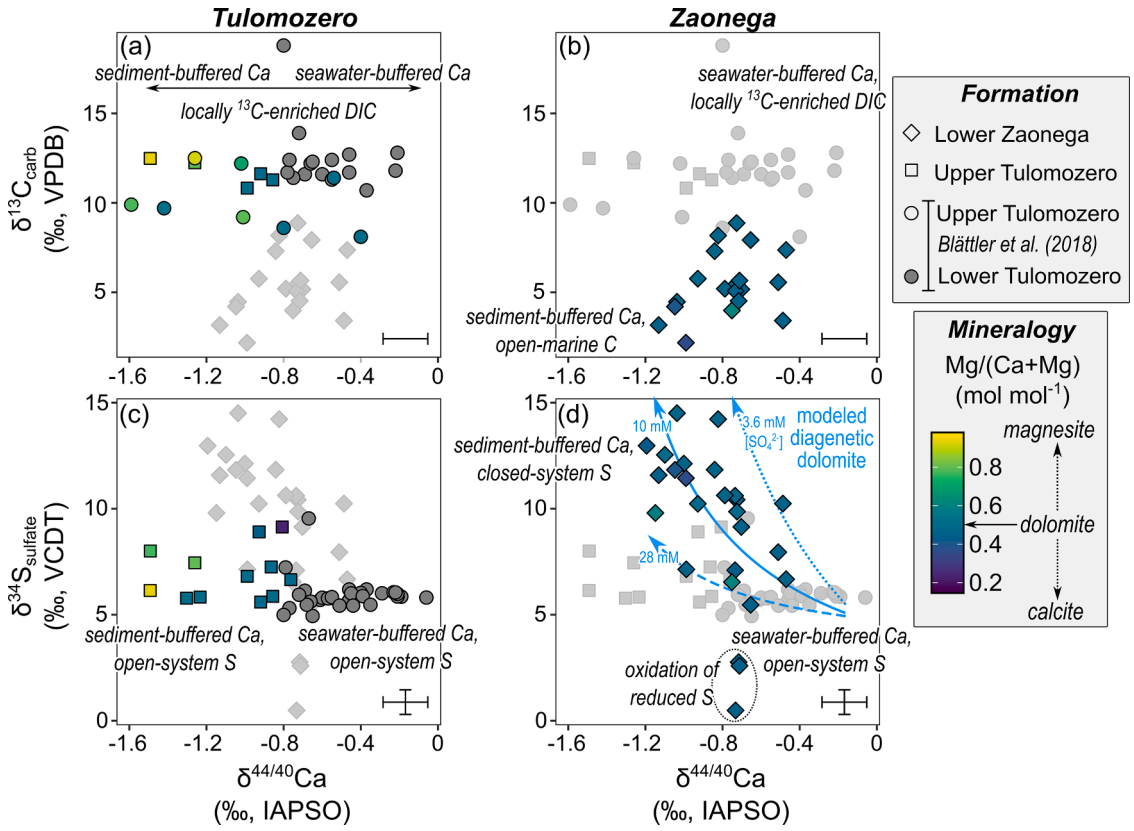

Fig. 3. Crossplots of $\delta^{13}C$ vs $\delta^{44/40}Ca$ for the Tulomozero Formation (a) and Zaonega Formation (b), and CAS $\delta^{34}S$ vs $\delta^{44/40}Ca$ for the Tulomozero Formation (c) and Zaonega Formation (d). $\delta^{13}C$ data are from Prave et al. (2022) excepting those marked by circles, which are from Blättler et al. (2018); dark gray circles are for magnesite-anhydrite in the lower Tulomozero Formation; in all panels, underlaid light gray symbols indicate data from the other formation. The blue lines in panel (d) are diagenetic dolomite trajectories generated using a marine carbonate diagenesis model (Ahm et al., 2018; Bryant et al., 2022) at variable seawater $[SO_4^{2-}]$ of 10 mM [Blättler et al. (2018) minimum constraint; solid], 28 mM (modern value; long dashes), and 3.6 mM (short dashes), showing that the changes in $\delta^{44/40}Ca$ and CAS $\delta^{34}S$ through the Zaonega Formation are broadly consistent with theoretical predictions for a transition from more seawater- to sediment-buffered early marine diagenesis (see methods for model parameterization details). The concurrent shift to lower $\delta^{13}C$ values is consistent with the sampling of a more open marine DIC pool (Geyman and Maloof, 2019). Error bars shown are long-term external reproducibility (±2σ) for carbonate standards. For $\delta^{13}C$, errors are smaller than the symbols.

Sr/(Ca+Mg) (median 0.14 × 10^{-3} mol mol^{-1}), and $\delta^{26}Mg$ (median −1.1‰) variability in dolomites of the Tulomozero Formation [which is accompanied by relative stasis in $\delta^{13}C$ (median +10.6‰) and CAS $\delta^{34}S$ (median +6.3‰) values; Fig. 3a, c] as a function of, 1) a continuum of seawater- to sediment-buffered early marine diagenesis in a sulfate-replete, organic-poor system, and/or 2) high but variable rates of carbonate precipitation and/or dolomitization, which can produce kinetic variations in the fractionation factor between mineral and solution (Mills et al., 2021). A sedimentary system dominated by advection of brines should have resulted in seawater-buffered (^{44}Ca-enriched) dolomitization. However, the same fluids could have supported rapid carbonate precipitation with large negative fractionations from solution, which complicates interpretation of the preserved $\delta^{44/40}Ca$ values.

The same two mechanisms have been invoked to explain widely varying $\delta^{44/40}Ca$ accompanied by invariant CAS $\delta^{34}S$ in brine-influenced shelf-facies dolomite from the Permian Capitan Reef Complex (Bryant et al., 2022). The Tulomozero Formation and Capitan Reef Complex shelf facies also have abundant seafloor precipitates and early marine cements (Brasier et al., 2011; Grotzinger and Knoll, 1995; Prave et al., 2022; Present et al., 2019). In both cases, the relatively invariant CAS $\delta^{34}S$ likely reflects plentiful sulfate supply from seawater during dolomitization. Therefore, like the Capitan Reef Complex shelf dolomite (Bryant et al., 2022; Present et al., 2019), the Tulomozero Formation carbonates likely retain CAS $\delta^{34}S$ values that are representative of contemporaneous seawater sulfate. Our CAS $\delta^{34}S$ values for the upper Tulomozero Formation are broadly consistent with the anhydrite $\delta^{34}S$ of the OPH and FAR-DEEP cores (Barkan et al., 2020; Blättler et al., 2018; Reuschel et al., 2012) but ~3‰ lower than the stratigraphically equivalent CAS $\delta^{34}S$ values (Reuschel et al., 2012) reported for the FAR-DEEP cores; this discrepancy might reflect regional differences in CAS preservation in the upper Tulomozero Formation.

4.2. Deposition and diagenesis of the Zaonega Formation

The upper Tulomozero Formation to lower Zaonega Formation interval captures a transgressive shift from shallow-marine environments to open and deeper-marine settings (Prave et al., 2022) (Fig. 4). This transition also likely prompted a shift from carbonate precipitation out of a locally ^{13}C-enriched shallow water DIC pool to an open-ocean DIC pool. Between depths of 2000–1900m, the median $\delta^{13}C$ value is +4.5‰ and decreases to a minimum of +2.2‰ up-section. In the same portion of the OPH core, we identify co-occurring shifts to lower $\delta^{44/40}Ca$ values (median −1.0‰) and higher CAS $\delta^{34}S$ (median +11.8‰), Sr/(Ca+Mg) (median 0.16 × 10^{-3} mol mol^{-1}), and $\delta^{26}Mg$ (median −1.0‰) values within the Zaonega Formation (Figs. 2, 3b, 4a). The $\delta^{44/40}Ca$ and Sr/(Ca+Mg) trends indicate that changes in the depositional environment caused a shift to dolomitization under more sediment-buffered conditions (Ahm et al., 2018; Blättler et al., 2015; Bryant et al., 2022), whilst the slight increase in $\delta^{26}Mg$ is consistent with increased Rayleigh distillation associated with prior dolomitization along a longer flow path. Within this interpretative framework, some of the shift in $\delta^{13}C$ values back toward 0‰ could have been driven by oxidation of OM

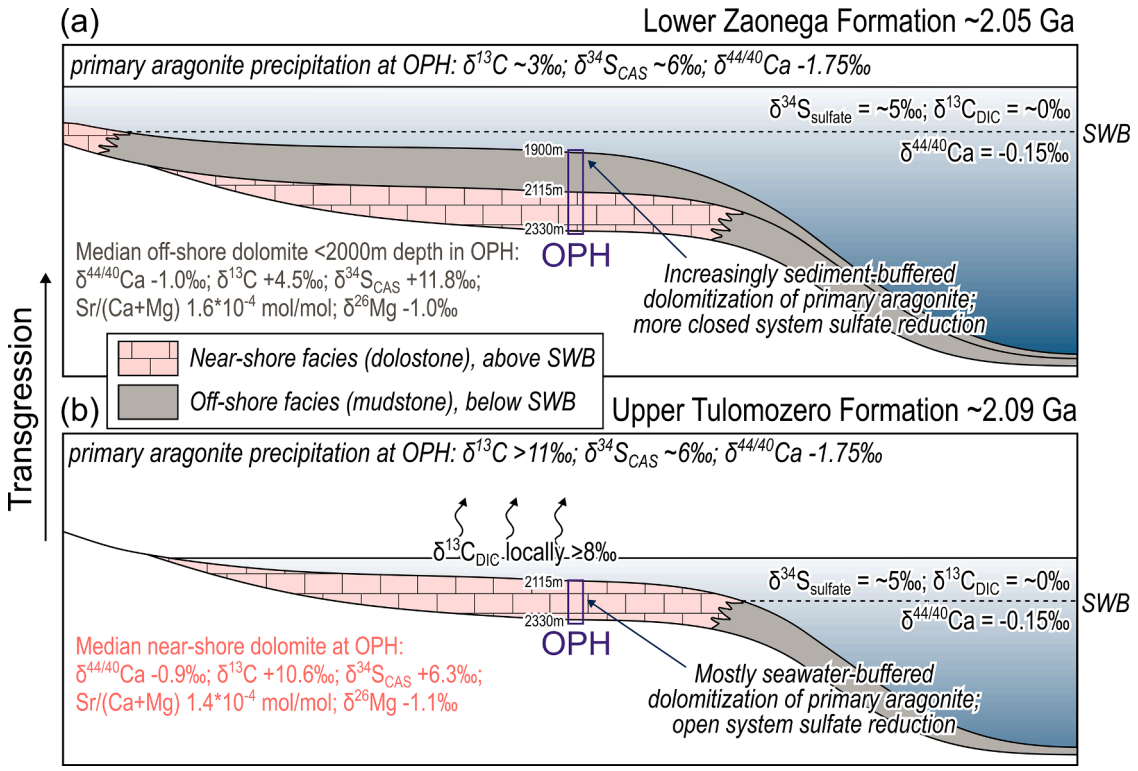

Fig. 4. Schematic interpretations of the environmental and associated diagenetic effects on dolomite-hosted geochemical indices discussed herein, for (a) the lower Zaonega Formation, and (b) the upper Tulomozero Formation, which together represent a marine transgression. 'SWB' stands for Storm Wave Base.

during diagenesis and incorporation of ^{13}C-depleted pore water DIC into diagenetic carbonates. However, the lack of $\delta^{13}C$ values <0‰ is more consistent with a progressive shift towards the sampling of open-ocean DIC rather than evolved pore-water DIC associated with OM oxidation.

With greater certainty, the $\delta^{44/40}Ca$ and Sr/(Ca+Mg) data allow us to attribute the shift to higher CAS $\delta^{34}S$ values to overprinting by simultaneous MSR and carbonate recrystallization in pore waters partially closed with respect to both calcium and sulfate. Although CAS concentrations do not negatively correlate with $\delta^{34}S$ values as anticipated for MSR, this could reflect much later loss of CAS (Fig. 2). Loss of CAS need not have affected residual $\delta^{34}S$ values (Gill et al., 2008), although the few anomalously low CAS $\delta^{34}S$ values (<5‰) likely indicate some late diagenetic remobilization of other sulfur pools (i.e., the dominant organic sulfur pool, or pyrite – as indicated by XAS data; Fig. 2). Pyrite in the Zaonega Formation immediately overlying the section studied here has $\delta^{34}S$ values ~20‰ lower relative to the CAS measured in this study (Paiste et al., 2020), which is consistent with prevailing closed-system MSR in sediment pore waters (Bryant et al., 2023a; Claypool, 2004; Halevy et al., 2023; Jorgensen, 1979; Pasquier et al., 2021), likely driven by the high initial OM content. Samples farther up section in the Zaonega Formation have been affected by pervasive late diagenetic or metamorphic overprinting of early diagenetic pyrite (Paiste et al., 2022, 2020). The apparent resistance of CAS $\delta^{34}S$ to late diagenetic overprinting, despite the co-occurrence of other sulfur pools (Fig. 2), could be related to the CAS being hosted in dolomite (Crockford et al., 2021), and is encouraging for the use of ancient CAS in past environmental reconstructions.

4.3. A consistent mode of early diagenetic CAS overprinting since the GOE

Dolomite in the lower Zaonega Formation bears strikingly similar geochemical behavior to the slope limestones of the Permian Capitan Reef (Bryant et al., 2022) and the partially dolomitized Miocene carbonates of the Clino core in the Bahamas (Murray et al., 2021). Inferred coeval seawater sulfate $\delta^{34}S$ values, constrained in each case from both sulfate evaporites and combined CAS $\delta^{34}S$ and $\delta^{44/40}Ca$ data, were ~21‰ (Murray et al., 2021), ~9‰ (Bryant et al., 2022; Present et al., 2019), and ~5‰ (Blättler et al., 2018; this study), during the deposition of the carbonates in the Clino core, Capitan Reef Complex, and Zaonega Formation, respectively. In the case of the Zaonega Formation, our estimate for coeval seawater is derived from data on the underlying Tulomozero Formation, i.e., we assume that seawater sulfate $\delta^{34}S$ did not evolve substantially prior to or during the deposition of the lower Zaonega Formation. This assumption is partially justified due to, 1) the high (>10 mM) seawater sulfate concentration inferred from the Tulomozero Formation and associated long residence time and low relative sensitivity of seawater sulfate $\delta^{34}S$ to biogeochemical perturbation (Blättler et al., 2018); 2) the limited variability of sulfate $\delta^{34}S$ throughout the Tulomozero Formation in the OPH core (Blättler et al., 2018; this study); and, 3) the low CAS $\delta^{34}S$ values and very high (seawater-buffered) $\delta^{44/40}Ca$ values at the base of the Zaonega Formation (e.g., 6.7‰ and −0.5‰, respectively, for the sample at 2104.5 m depth in the OPH core), which are consistent with a seawater sulfate $\delta^{34}S$ value close to 5‰ (Barkan et al., 2020).

In each of the Clino core carbonates, Capitan Reef Complex, and Zaonega Formation, collectively spanning 2 Gyr, positive offsets in CAS $\delta^{34}S$ values of ~10‰ relative to inferred coeval seawater negatively correlate with low $\delta^{44/40}Ca$ values (Fig. 5; Fig. S4). The negative correlation between CAS $\delta^{34}S$ and $\delta^{44/40}Ca$ in these cases likely indicates that recrystallization/dolomitization of primary carbonate minerals overlapped in time/space with MSR-driven ^{34}S-enrichment of residual pore water sulfate. Recrystallization in more closed conditions [e.g., farther below the sediment-water interface; (Ahm et al., 2018)] results in lower, more sediment-buffered $\delta^{44/40}Ca$ values and more elevated CAS $\delta^{34}S$. These observations collectively demonstrate that pore fluid changes driven by MSR and early diagenetic recrystallization have had the potential to influence carbonate geochemistry since at least the GOE – particularly in slope settings. Considering these findings, other

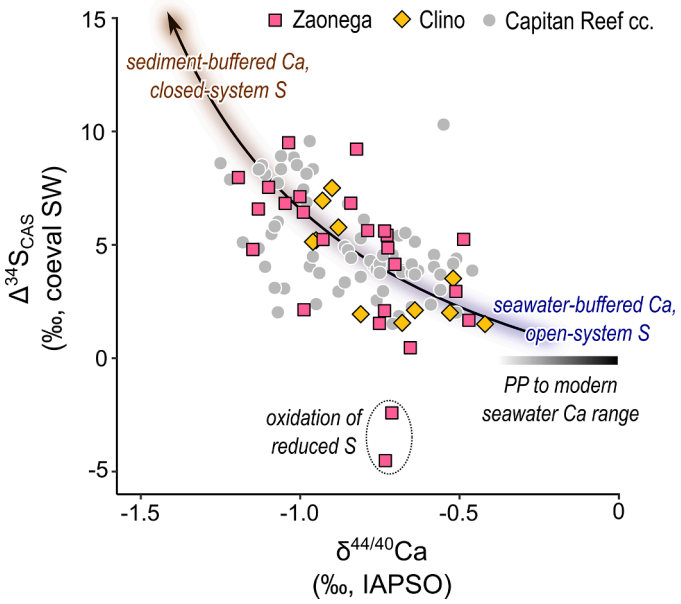

Fig. 5. Crossplot of $\delta^{44/40}$Ca and offsets (Δ^{34}S) of CAS δ^{34}S relative to inferred coeval seawater (SW), for dolomite from the lower Zaonega Formation (this study), calcite from shelf slope facies in the Permian Capitan Reef (Bryant et al., 2022; Present et al., 2019), and partially dolomitized Miocene carbonates from slope facies in the Clino core in the Bahamas (Murray et al., 2021). Broadly, the negative correlation between the variables in diagenetic carbonates (Fig. S4), visualized with the arrow, is best explained by synchronous MSR and recrystallization/dolomitization in a range of seawater- to sediment-buffered conditions that commonly exist in shelf slope settings. Changes in the slope of the Ca-CAS correlation can be driven by changes in the relative rates of MSR and recrystallization, or the concentrations of Ca and sulfate in seawater (Bryant et al., 2022). 'PP' = Paleoproterozoic.

down-core variations in CAS δ^{34}S used for reconstruction of oceanic sulfate concentrations (Algeo et al., 2015; Planavsky et al., 2012), should also be evaluated with contextual information from diagenetic proxies (e.g., $\delta^{44/40}$Ca) and sedimentary facies. Most studies using CAS δ^{34}S to reconstruct ocean sulfate concentrations specifically target carbonate-rich sedimentary rocks (Fike et al., 2006; Planavsky et al., 2012), which are not directly comparable to the carbonate-poor Zaonega Formation samples. Recent evidence suggests that although CAS δ^{34}S values of carbonate rocks do not always faithfully preserve the δ^{34}S of contemporaneous seawater sulfate (Bryant et al., 2022; Murray et al., 2021; Present et al., 2019; Richardson et al., 2021), carbonates deposited shoreward of the outer shelf (Fig. 4) are more likely to do so.

4.4. Implications for the GOE

To interpret the LJE at face value, the global ocean dissolved inorganic carbon (DIC) pool would have needed to be remarkably enriched in ^{13}C by sustained OM burial, which, in turn, would imply an enormous magnitude for the GOE and, presumably, subsequent O_2 drawdown (Bekker and Holland, 2012; Karhu and Holland, 1996). However, doubt around the global nature of the LJE has lingered for decades (Schidlowski et al., 1976), and now it seems likely that the oceanic DIC pool was not uniformly mixed across the LJE: while shallow-marine facies record the full LJE, contemporaneous deeper marine sedimentary facies tend to record a small (or absent) LJE (Hodgskiss et al., 2023; Prave et al., 2022). Similar trends have been observed in the modern Bahamas (Geyman and Maloof, 2021) and in the Triassic of southern China (Meyer et al., 2011), albeit with smaller magnitude ^{13}C enrichments, suggesting that locally ^{13}C-enriched DIC in shallow depositional settings may constitute a significant driver of elevated δ^{13}C values in the geologic record. The modern and Triassic analogs don't explain the duration of the LJE, nor the rarity of similar magnitude excursions in the geologic record, both of which require further study. Recent work has postulated that methanogenesis and partial methane loss to the atmosphere could have driven the production of LJE signals in shallow marine settings, with the LJE being terminated by respiration displacing methanogenesis as the dominant OM-remineralization process (Sumner, 2024). Regardless of the driving mechanism, if the LJE almost exclusively constituted a shallow-water phenomenon (Prave et al., 2022), it could have been produced by substantially less OM burial than traditionally interpreted and resulted in comparatively limited ocean-atmospheric oxidation.

Despite the uncertainty associated with the extent of the GOE, a degree of oxygenation was necessary to halt S-MIF production (Farquhar et al., 2000) and produce a seawater sulfate reservoir of >10 mM at ~2 Ga (Blättler et al., 2018). However, against the backdrop of more modest Earth system oxygenation proposed here based on new interpretations of the records of δ^{13}C and δ^{34}S, a surficial O_2 reservoir decline by a factor of 10 or more in the aftermath of the LJE seems less viable. Given our results, CAS δ^{34}S data throughout the Paleoproterozoic (Fig. 1) require extensive reassessment before they can be employed as evidence of a surficial oxidant buildup and drawdown (Bachan and Kump, 2015; Planavsky et al., 2012). In the Onega Basin, the rising CAS δ^{34}S trend clearly reflects increasing early diagenetic ^{34}S-enrichment of CAS in the aftermath of the GOE, driven by changes in depositional environment and diagenetic style. As such, this region provides no substantive evidence that marine sulfate and atmospheric oxygen were drawn down in the immediate aftermath of the LJE (Bachan and Kump, 2015; Planavsky et al., 2012).

A growing number of studies indicate that the diagenetic proxies $\delta^{44/40}$Ca and Sr/(Ca+Mg) are reliable tools for testing the preservation quality of CAS δ^{34}S in marine sediments of all ages (Bryant et al., 2022; Higgins et al., 2018; Murray et al., 2021). Thus, there is great scope for investigating CAS δ^{34}S in this context to decipher global oxygenation across the GOE. To accomplish this effectively, it will be necessary to find and investigate sedimentary strata whose depositional and diagenetic histories are more conducive to CAS abundance and δ^{34}S preservation of coeval seawater. One candidate is the Paleoproterozoic Francevillian succession (Gabon), whose deeper-water depositional setting (Mayika et al., 2020) might have favored minimal overprinting of CAS.

5. Conclusions

In this study, we used a holistic multi-proxy approach to tease apart the influences of diagenetic/depositional factors on geochemical records of carbon (carbonate δ^{13}C) and sulfur (CAS δ^{34}S) cycle behavior in the Onega Basin following the GOE. Our main conclusions are as follows:

(1) A rising CAS δ^{34}S trend in the Zaonega Formation, that could ordinarily be interpreted as evidence of sulfate reservoir collapse, is accompanied by a stark decrease in $\delta^{44/40}$Ca and an increase in Sr/(Ca+Mg). These observations suggest that the style of carbonate diagenesis shifted from seawater- to sediment-buffered, and that the CAS δ^{34}S trend is likely the result of increased closed-system MSR overprinting primary CAS δ^{34}S. As such, these data cannot be used to test theories of sulfate reservoir collapse after the GOE.

(2) The negative correlation between $\delta^{44/40}$Ca and CAS δ^{34}S is comparable to those observed in slope sediments from the Permian and Miocene. We interpret this to mean that a consistent mode of CAS δ^{34}S overprinting has existed since the GOE. We urge caution in the use of down-core variations in CAS δ^{34}S to reconstruct sulfur cycling in deep time, although we note that $\delta^{44/40}$Ca, Sr/(Ca+Mg), and facies analysis can effectively be used to filter out non-primary CAS δ^{34}S values.

(3) Given our results, and recent suggestions that the LJE is a shallow-water phenomenon, we suggest that evidence is lacking for a surficial O_2 reservoir decline by a factor of 10 or more in the aftermath of the LJE. More work is required to accurately reconstruct oxygenation in this crucial slice of geologic time, but we suggest that paired use of $\delta^{44/40}$Ca and CAS δ^{34}S provides a promising path forward.

CRediT authorship contribution statement

Roger N. Bryant: Writing – review & editing, Writing – original draft, Visualization, Project administration, Methodology, Investigation, Formal analysis, Data curation, Conceptualization. **Jordan P. Todes:** Writing – review & editing, Writing – original draft, Investigation, Formal analysis. **Jocelyn A. Richardson:** Writing – review & editing, Writing – original draft, Investigation, Formal analysis. **Tara C. Kalia:** Writing – review & editing, Investigation. **Anthony R. Prave:** Writing – review & editing, Investigation, Funding acquisition. **Aivo Lepland:** Writing – review & editing, Investigation, Funding acquisition. **Kalle Kirsimäe:** Writing – review & editing, Investigation, Funding acquisition. **Clara L. Blättler:** Writing – review & editing, Supervision, Resources, Project administration, Funding acquisition, Formal analysis, Data curation, Conceptualization.

Declaration of competing interest

The authors declare that they have no known competing financial interests or personal relationships that could have appeared to influence the work reported in this paper.

Acknowledgments

We thank editor Huiming Bao, Jiarui Liu, and three anonymous reviewers for their insightful comments that greatly improved this work. Acknowledgement is made to the donors of the American Chemical Society Petroleum Research Fund for partial support of this research (ACS-PRF# 62442-DNI2 to CLB). CLB acknowledges support from the NSF [(EAR) 2339237]. JPT was supported by an NSF GRF. TCK was supported by a summer research grant from the Metcalf Program (University of Chicago). KK, AL, AP were supported by Estonian Science Foundation grant PRG2123. Use of the Stanford Synchrotron Radiation Lightsource, SLAC National Accelerator Laboratory, is supported by the U.S. Department of Energy, Office of Science, Office of Basic Energy Sciences under Contract No DE-AC02–76SF00515. The SSRL Structural Molecular Biology Program is supported by the DOE Office of Biological and Environmental Research, and by the National Institutes of Health, National Institute of General Medical Sciences (P30GM133894). The contents of this publication are solely the responsibility of the authors and do not necessarily represent the official views of NIGMS or NIH.

Supplementary materials

Supplementary material associated with this article can be found, in the online version, at doi:10.1016/j.epsl.2024.119113.

Data availability

We include all data as additional supplemental files to be made available with the online version of the article.

References

Ahm, A.S.C., Bjerrum, C.J., Blättler, C.L., Swart, P.K., Higgins, J.A., 2018. Quantifying early marine diagenesis in shallow-water carbonate sediments. Geochim. Cosmochim. Acta 236, 140–159. https://doi.org/10.1016/j.gca.2018.02.042.

Algeo, T.J., Luo, G.M., Song, H.Y., Lyons, T.W., Canfield, D.E., 2015. Reconstruction of secular variation in seawater sulfate concentrations. Biogeosciences. 12, 2131–2151. https://doi.org/10.5194/bg-12-2131-2015.

Anzures, B.A., Parman, S.W., Milliken, R.E., Lanzirotti, A., Newville, M., 2020. XANES spectroscopy of sulfides stable under reducing conditions. Am. Mineral. 105, 375–381. https://doi.org/10.2138/am-2020-7146.

Bachan, A., Kump, L.R., 2015. The rise of oxygen and siderite oxidation during the Lomagundi Event. Proc. Natl. Acad. Sci. 112, 6562–6567. https://doi.org/10.1073/pnas.1422319112.

Banner, J.L., 1995. Application of the trace element and isotope geochemistry of strontium to studies of carbonate diagenesis. Sedimentology 42, 805–824. https://doi.org/10.1111/j.1365-3091.1995.tb00410.x.

Banner, J.L., Hanson, G.N., 1990. Calculation of simultaneous isotopic and trace element variations during water-rock interaction with applications to carbonate diagenesis. Geochim. Cosmochim. Acta 54, 3123–3137. https://doi.org/10.1016/0016-7037(90)90128-8.

Barkan, Y., Paris, G., Webb, S.M., Adkins, J.F., Halevy, I., 2020. Sulfur isotope fractionation between aqueous and carbonate-associated sulfate in abiotic calcite and aragonite. Geochim. Cosmochim. Acta 280, 317–339. https://doi.org/10.1016/j.gca.2020.03.022.

Bekker, A., Holland, H.D., 2012. Oxygen overshoot and recovery during the early Paleoproterozoic. Earth. Planet. Sci. Lett. 317–318, 295–304. https://doi.org/10.1016/j.epsl.2011.12.012.

Blättler, C.L., Claire, M.W., Prave, A.R., Kirsimäe, K., Higgins, J.A., Medvedev, P.V., Romashkin, A.E., Rychanchik, D.V., Zerkle, A.L., Paiste, K., Kreitsmann, T., Millar, I. L., Hayles, J.A., Bao, H., Turchyn, A.V., Warke, M.R., Lepland, A., 2018. Two-billion-year-old evaporites capture Earth's great oxidation. Science (1979) 360, 320–323. https://doi.org/10.1126/science.aar2687.

Blättler, C.L., Miller, N.R., Higgins, J.A., 2015. Mg and Ca isotope signatures of authigenic dolomite in siliceous deep-sea sediments. Earth. Planet. Sci. Lett. 419, 32–42. https://doi.org/10.1016/j.epsl.2015.03.006.

Bradbury, H.J., Turchyn, A.V., 2018. Calcium isotope fractionation in sedimentary pore fluids from ODP Leg 175: resolving carbonate recrystallization. Geochim. Cosmochim. Acta 236, 121–139. https://doi.org/10.1016/j.gca.2018.01.040.

Brasier, A.T., Fallick, A.E., Prave, A.R., Melezhik, V.A., Lepland, A., 2011. Coastal sabkha dolomites and calcitised sulphates preserving the Lomagundi-Jatuli carbon isotope signal. Precambrian. Res. 189, 193–211. https://doi.org/10.1016/j.precamres.2011.05.011.

Bryant, R.N., Houghton, J.L., Jones, C., Pasquier, V., Halevy, I., Fike, D.A., 2023a. Deconvolving microbial and environmental controls on marine sedimentary pyrite sulfur isotope ratios. Science (1979) 382, 912–915. https://doi.org/10.1126/science.adg6103.

Bryant, R.N., Present, T.M., Ahm, A.-S.C., McClelland, H.-L.O., Razionale, D., Blättler, C. L., 2022. Early diagenetic constraints on Permian seawater chemistry from the Capitan Reef. Geochim. Cosmochim. Acta 328, 1–18. https://doi.org/10.1016/j.gca.2022.04.027.

Bryant, R.N., Richardson, J.A., Kalia, T.C., Gros, O., Lopez-Garriga, J., Blättler, C.L., 2023b. Inorganic sulfate–based signatures of chemosymbiosis in modern infaunal lucinids. Geology. 51, 1022–1026. https://doi.org/10.1130/G51353.1.

Canfield, D.E., Farquhar, J., 2009. Animal evolution, bioturbation, and the sulfate concentration of the oceans. Proc. Natl. Acad. Sci. 106, 8123–8127. https://doi.org/10.1073/pnas.0902037106.

Claypool, G.E., 2004. Ventilation of marine sediments indicated by depth profiles of pore water sulfate and δ34S. Geochem. Soc. Spec. Publ. 9, 59–65. https://doi.org/10.1016/S1873-9881(04)80007-5.

Cloud, P., 1973. Paleoecological significance of the banded iron-formation. Econ. Geol. 68, 1135–1143. https://doi.org/10.2113/gsecongeo.68.7.1135.

Coplen, T.B., 1995. Discontinuance of SMOW and PDB. Nature 375. https://doi.org/10.1038/375285a0, 285–285.

Črne, A., Melezhik, V., Lepland, A., Fallick, A.E., Prave, A.R., Brasier, A.T., 2014. Petrography and geochemistry of carbonate rocks of the Paleoproterozoic Zaonega Formation, Russia: documentation of 13C-depleted non-primary calcite. Precambrian. Res. 240, 79–93. https://doi.org/10.1016/j.precamres.2013.10.005.

Crockford, P.W., Kunzmann, M., Blättler, C.L., Kalderon-Asael, B., Murphy, J.G., Ahm, A. S., Sharoni, S., Halverson, G.P., Planavsky, N.J., Halevy, I., Higgins, J.A., 2021. Reconstructing Neoproterozoic seawater chemistry from early diagenetic dolomite. Geology. 49, 442–446. https://doi.org/10.1130/G48213.1.

Ding, T., Bai, R., Li, Y., Wan, D., Zou, X., Zhang, Q., 1999. Determination of the absolute32S/34S ratio of IAEA-S-1 reference material and V-CDT sulfur isotope standard. Sci. China Ser. D. Earth. Sci. 42, 45–51. https://doi.org/10.1007/BF02878497.

Fantle, M.S., DePaolo, D.J., 2007. Ca isotopes in carbonate sediment and pore fluid from ODP Site 807A: the Ca2+(aq)–calcite equilibrium fractionation factor and calcite recrystallization rates in Pleistocene sediments. Geochim. Cosmochim. Acta 71, 2524–2546. https://doi.org/10.1016/j.gca.2007.03.006.

Farquhar, J., Bao, H., Thiemens, M., 2000. Atmospheric influence of Earth's earliest sulfur cycle. Science (1979) 289, 756–758. https://doi.org/10.1126/science.289.5480.756.

Farquhar, J., Wing, B.A., 2003. Multiple sulfur isotopes and the evolution of the atmosphere. Earth. Planet. Sci. Lett. 213, 1–13. https://doi.org/10.1016/S0012-821X(03)00296-6.

Fike, D.A., Bradley, A.S., Rose, C.V., 2015. Rethinking the ancient sulfur cycle. Annu Rev. Earth. Planet. Sci. 43, 593–622. https://doi.org/10.1146/annurev-earth-060313-054802.

Fike, D.A., Grotzinger, J.P., Pratt, L.M., Summons, R.E., 2006. Oxidation of the Ediacaran ocean. Nature 444, 744–747. https://doi.org/10.1038/nature05345.

Gallagher, K.L., Dupraz, C., Visscher, P.T., 2014. Two opposing effects of sulfate reduction on carbonate precipitation in normal marine, hypersaline, and alkaline environments: comment. Geology. https://doi.org/10.1130/G34639C.1.

Galy, A., Yoffe, O., Janney, P.E., Williams, R.W., Cloquet, C., Alard, O., Halicz, L., Wadhwa, M., Hutcheon, I.D., Ramon, E., Carignan, J., 2003. Magnesium isotope heterogeneity of the isotopic standard SRM980 and new reference materials for magnesium-isotope-ratio measurements. J. Anal. At. Spectrom. 18, 1352. https://doi.org/10.1039/b309273a.

Geyman, E.C., Maloof, A.C., 2021. Facies control on carbonate δ13C on the Great Bahama Bank. Geology. 49, 1049–1054. https://doi.org/10.1130/G48862.1.

Geyman, E.C., Maloof, A.C., 2019. A diurnal carbon engine explains 13C-enriched carbonates without increasing the global production of oxygen. Proc. Natl. Acad. Sci. U S. A 116, 24433–24439. https://doi.org/10.1073/pnas.1908783116.

Gill, B.C., Lyons, T.W., Frank, T.D., 2008. Behavior of carbonate-associated sulfate during meteoric diagenesis and implications for the sulfur isotope paleoproxy. Geochim. Cosmochim. Acta 72, 4699–4711. https://doi.org/10.1016/j.gca.2008.07.001.

Grotzinger, J.P., Knoll, A.H., 1995. Anomalous carbonate precipitates: is the Precambrian the key to the Permian? Palaios. 10, 578–596. https://doi.org/10.2307/3515096.

Halevy, I., Fike, D.A., Pasquier, V., Bryant, R.N., Wenk, C.B., Turchyn, A.V., Johnston, D. T., Claypool, G.E., 2023. Sedimentary parameters control the sulfur isotope composition of marine pyrite. Science (1979) 382, 946–951. https://doi.org/10.1126/science.adh1215.

Hannah, J., Stein, H., Zimmerman, A., Yang, G., Melezhik, V., Filippov, M., Turgeon, S., Creaser, R., 2008. *Re*-Os geochronology of shungite: a 2.05 Ga fossil oil field in Karelia. In: The 33rd International Geological Congress. Oslo.

Hardisty, D.S., Lu, Z., Bekker, A., Diamond, C.W., Gill, B.C., Jiang, G., Kah, L.C., Knoll, A. H., Loyd, S.J., Osburn, M.R., Planavsky, N.J., Wang, C., Zhou, X., Lyons, T.W., 2017. Perspectives on Proterozoic surface ocean redox from iodine contents in ancient and recent carbonate. Earth. Planet. Sci. Lett. 463, 159–170. https://doi.org/10.1016/j.epsl.2017.01.032.

Higgins, J.A., Blättler, C.L., Lundstrom, E.A., Santiago-Ramos, D.P., Akhtar, A.A., Crüger Ahm, A.S., Bialik, O., Holmden, C., Bradbury, H., Murray, S.T., Swart, P.K., 2018. Mineralogy, early marine diagenesis, and the chemistry of shallow-water carbonate sediments. Geochim. Cosmochim. Acta 220, 512–534. https://doi.org/10.1016/j.gca.2017.09.046.

Hodgskiss, M.S.W., Crockford, P.W., Turchyn, A.V., 2023. Deconstructing the Lomagundi-Jatuli carbon isotope excursion. Annu Rev. Earth. Planet. Sci. 51. https://doi.org/10.1146/annurev-earth-031621-071250.

Holland, H.D., 2002. Volcanic gases, black smokers, and the great oxidation event. Geochim. Cosmochim. Acta 66, 3811–3826. https://doi.org/10.1016/S0016-7037(02)00950-X.

Jacobson, A.D., Holmden, C., 2008. δ44Ca evolution in a carbonate aquifer and its bearing on the equilibrium isotope fractionation factor for calcite. Earth. Planet. Sci. Lett. 270, 349–353. https://doi.org/10.1016/j.epsl.2008.03.039.

Jorgensen, B.B., 1979. A theoretical model of the stable sulfur isotope distribution in marine sediments. Geochim. Cosmochim. Acta 43, 363–374. https://doi.org/10.1016/0016-7037(79)90201-1.

Kampschulte, A., Strauss, H., 2004. The sulfur isotopic evolution of Phanerozoic seawater based on the analysis of structurally substituted sulfate in carbonates. Chem Geol 204, 255–286. https://doi.org/10.1016/j.chemgeo.2003.11.013.

Karhu, J.A., Holland, H.D., 1996. Carbon isotopes and the rise of atmospheric oxygen. Geology. 24, 867. https://doi.org/10.1130/0091-7613(1996)024<0867:CIATRO>2.3.CO;2.

Krupenik, V., Sveshnikova, K., 2011. Correlation of Onega parametric borehole section with the reference sections in the Onega structure. In: Glushanin, L., Sharov, N., Shchiptsov, V. (Eds.), Palaeoproterozoic Onega Structure (Geology, Tectonics, Deep Structure and Mineralogeny). Karelian Research Centre, Russian Academy of Sciences, Petrozavodsk, pp. 190–195.

Kurtz, A.C., Kump, L.R., Arthur, M.A., Zachos, J.C., Paytan, A., 2003. Early Cenozoic decoupling of the global carbon and sulfur cycles. Paleoceanography 18. https://doi.org/10.1029/2003PA000908.

Lau, K.V., Hardisty, D.S., 2022. Modeling the impacts of diagenesis on carbonate paleoredox proxies. Geochim. Cosmochim. Acta 337, 123–139. https://doi.org/10.1016/J.GCA.2022.09.021.

Manceau, A., Nagy, K.L., 2012. Quantitative analysis of sulfur functional groups in natural organic matter by XANES spectroscopy. Geochim. Cosmochim. Acta 99, 206–223. https://doi.org/10.1016/j.gca.2012.09.033.

Mayika, K.B., Moussavou, M., Prave, A.R., Lepland, A., Mbina, M., Kirsimäe, K., 2020. The Paleoproterozoic Francevillian succession of Gabon and the Lomagundi-Jatuli event. Geology. 48, 1099–1104. https://doi.org/10.1130/g47651.1.

Melezhik, V.A., Fallick, A.E., 1996. A widespread positive δ13 C carb anomaly at around 2.33-2.06 Ga on the Fennoscandian Shield: a paradox? Terra Nova 8, 141–157. https://doi.org/10.1111/j.1365-3121.1996.tb00738.x.

Melezhik, V.A., Fallick, A.E., Medvedev, P.V., Makarikhin, V.V., 2001. Palaeoproterozoic magnesite: lithological and isotopic evidence for playa/sabkha environments. Sedimentology 48, 379–397. https://doi.org/10.1046/j.1365-3091.2001.00369.x.

Meyer, K.M., Yu, M., Jost, A.B., Kelley, B.M., Payne, J.L., 2011. δ13C evidence that high primary productivity delayed recovery from end-Permian mass extinction. Earth. Planet. Sci. Lett. 302, 378–384. https://doi.org/10.1016/j.epsl.2010.12.033.

Mills, J.V., DePaolo, D.J., Lammers, L.N., 2021. The influence of Ca:CO3 stoichiometry on Ca isotope fractionation: implications for process-based models of calcite growth. Geochim. Cosmochim. Acta 298, 87–111. https://doi.org/10.1016/j.gca.2021.01.016.

Murray, S.T., Higgins, J.A., Holmden, C., Lu, C., Swart, P.K., 2021. Geochemical fingerprints of dolomitization in Bahamian carbonates: evidence from sulphur, calcium, magnesium and clumped isotopes. Sedimentology 68, 1–29. https://doi.org/10.1111/sed.12775.

Ovchinnikova, G.V., Kuznetsov, A.B., Melezhik, V.A., Gorokhov, I.M., Vasil'eva, I.M., Gorokhovskii, B.M., 2007. Pb-Pb age of Jatulian carbonate rocks: the Tulomozero Formation of southeast Karelia. Stratigr. Geol. Correlat. 15, 359–372. https://doi.org/10.1134/S0869593807040028.

Paiste, K., Fike, D.A., Kirsimäe, K., Jones, C., Lepland, A., 2022. Testing the global significance of the sulfur isotope record of the ca. 2.0 Ga Zaonega Formation: a micro-scale S isotope investigation. Geochim. Cosmochim. Acta 331, 86–104. https://doi.org/10.1016/J.GCA.2022.05.021.

Paiste, K., Pellerin, A., Zerkle, A.L., Kirsimäe, K., Prave, A.R., Romashkin, A.E., Lepland, A., 2020. The pyrite multiple sulfur isotope record of the 1.98 Ga Zaonega Formation: evidence for biogeochemical sulfur cycling in a semi-restricted basin. Earth. Planet. Sci. Lett. 534, 116092. https://doi.org/10.1016/J.EPSL.2020.116092.

Paris, G., Adkins, J.F., Sessions, A.L., Webb, S.M., Fischer, W.W., 2014. Neoarchean carbonate-associated sulfate records positive $\Delta^{33}S$ anomalies. Science (1979) 346, 739–741. https://doi.org/10.1126/science.1258211.

Paris, G., Sessions, A.L., Subhas, A.V., Adkins, J.F., 2013. MC-ICP-MS measurement of δ34S and Δ33S in small amounts of dissolved sulfate. Chem Geol 345, 50–61. https://doi.org/10.1016/j.chemgeo.2013.02.022.

Partin, C.A., Bekker, A., Planavsky, N.J., Scott, C.T., Gill, B.C., Li, C., Podkovyrov, V., Maslov, A., Konhauser, K.O., Lalonde, S.V., Love, G.D., Poulton, S.W., Lyons, T.W., 2013. Large-scale fluctuations in Precambrian atmospheric and oceanic oxygen levels from the record of U in shales. Earth. Planet. Sci. Lett. 369–370, 284–293. https://doi.org/10.1016/j.epsl.2013.03.031.

Pasquier, V., Bryant, R.N., Fike, D.A., Halevy, I., 2021. Strong local, not global, controls on marine pyrite sulfur isotopes. Sci. Adv. 7. https://doi.org/10.1126/sciadv.abb7403 eabb7403.

Planavsky, N.J., Bekker, A., Hofmann, A., Owens, J.D., Lyons, T.W., 2012. Sulfur record of rising and falling marine oxygen and sulfate levels during the Lomagundi event. Proc. Natl. Acad. Sci. 109, 18300–18305. https://doi.org/10.1073/pnas.1120387109.

Prave, A.R., Kirsimäe, K., Lepland, A., Fallick, A.E., Kreitsmann, T., Deines, Y.E., Romashkin, A.E., Rychanchik, D.V., Medvedev, P.V., Moussavou, M., Bakakas, K., Hodgskiss, M.S.W., 2022. The grandest of them all: the Lomagundi–Jatuli Event and Earth's oxygenation. J. Geol. Soc. London. 179. https://doi.org/10.1144/jgs2021-036 jgs2021-036.

Present, T.M., Gutierrez, M., Paris, G., Kerans, C., Grotzinger, J.P., Adkins, J.F., 2019. Diagenetic controls on the isotopic composition of carbonate-associated sulphate in the Permian Capitan Reef Complex, West Texas. Sedimentology 66, 2605–2626. https://doi.org/10.1111/sed.12615.

Present, T.M., Paris, G., Burke, A., Fischer, W.W., Adkins, J.F., 2015. Large Carbonate Associated Sulfate isotopic variability between brachiopods, micrite, and other sedimentary components in Late Ordovician strata. Earth. Planet. Sci. Lett. 432, 187–198. https://doi.org/10.1016/j.epsl.2015.10.005.

Ravel, B., Newville, M., 2005. ATHENA, ARTEMIS, HEPHAESTUS: data analysis for X-ray absorption spectroscopy using IFEFFIT. J. Synchrotron Radiat. Int. Union Crystallogr. 537–541. https://doi.org/10.1107/S0909049505012719.

Razionale, D., Bryant, R.N., Blättler, C.L., 2022. Adapting automated instrumentation for high-throughput calcium isotope measurements by multi-collector inductively coupled plasma mass spectrometry. Rapid Commun. Mass Spectrom. 36, e9249. https://doi.org/10.1002/rcm.9249.

Rennie, V.C.F., Turchyn, A.v., 2014. The preservation of δSSO434 and δOSO418 in carbonate-associated sulfate during marine diagenesis: a 25 Myr test case using marine sediments. Earth. Planet. Sci. Lett. 395, 13–23. https://doi.org/10.1016/j.epsl.2014.03.025.

Reuschel, M., Melezhik, V.A., Whitehouse, M.J., Lepland, A., Fallick, A.E., Strauss, H., 2012. Isotopic evidence for a sizeable seawater sulfate reservoir at 2.1Ga. Precambrian. Res. 192–195, 78–88. https://doi.org/10.1016/j.precamres.2011.10.013.

Richardson, J.A., Keating, C., Lepland, A., Hints, O., Bradley, A.S., Fike, D.A., 2019a. Silurian records of carbon and sulfur cycling from Estonia: the importance of depositional environment on isotopic trends. Earth. Planet. Sci. Lett. 512, 71–82. https://doi.org/10.1016/j.epsl.2019.01.055.

Richardson, J.A., Lepland, A., Hints, O., Prave, A.R., Gilhooly, W.P., Bradley, A.S., Fike, D.A., 2021. Effects of early marine diagenesis and site-specific depositional controls on carbonate-associated sulfate: insights from paired S and O isotopic analyses. Chem. Geol. 584, 120525. https://doi.org/10.1016/j.chemgeo.2021.120525.

Richardson, J.A., Newville, M., Lanzirotti, A., Webb, S.M., Rose, C.V., Catalano, J.G., Fike, D.A., 2019b. Depositional and diagenetic constraints on the abundance and spatial variability of carbonate-associated sulfate. Chem. Geol. 523, 59–72. https://doi.org/10.1016/j.chemgeo.2019.05.036.

Riechelmann, S., Mavromatis, V., Buhl, D., Dietzel, M., Immenhauser, A., 2020. Controls on formation and alteration of early diagenetic dolomite: a multi-proxy δ44/40Ca, δ26Mg, δ18O and δ13C approach. Geochim. Cosmochim. Acta 283, 167–183. https://doi.org/10.1016/j.gca.2020.06.010.

Schidlowski, M., Eichmann, R., Junge, C.E., 1976. Carbon isotope geochemistry of the Precambrian Lomagundi carbonate province, Rhodesia. Geochim. Cosmochim. Acta 40, 449–455. https://doi.org/10.1016/0016-7037(76)90010-7.

Schidlowski, M., Eichmann, R., Junge, C.E., 1975. Precambrian sedimentary carbonates: carbon and oxygen isotope geochemistry and implications for the terrestrial oxygen budget. Precambrian. Res. 2, 1–69. https://doi.org/10.1016/0301-9268(75)90018-2.

Scott, C., Wing, B.A., Bekker, A., Planavsky, N.J., Medvedev, P., Bates, S.M., Yun, M., Lyons, T.W., 2014. Pyrite multiple-sulfur isotope evidence for rapid expansion and contraction of the early Paleoproterozoic seawater sulfate reservoir. Earth. Planet. Sci. Lett. 389, 95–104. https://doi.org/10.1016/j.epsl.2013.12.010.

Sumner, D.Y., 2024. Oxygenation of Earth's atmosphere induced metabolic and ecologic transformations recorded in the Lomagundi-Jatuli carbon isotopic excursion. Appl. Environ. Microbiol. 90. https://doi.org/10.1128/aem.00093-24.

Teichert, B.M.A., Gussone, N., Torres, M.E., 2009. Controls on calcium isotope fractionation in sedimentary porewaters. Earth. Planet. Sci. Lett. 279, 373–382. https://doi.org/10.1016/j.epsl.2009.01.011.

Uveges, B.T., Izon, G., Ono, S., Beukes, N.J., Summons, R.E., 2023. Reconciling discrepant minor sulfur isotope records of the Great Oxidation Event. Nat. Commun. 14, 1–12. https://doi.org/10.1038/s41467-023-35820-w, 2023 14:1.

Webb, S.M., 2005. SIXpack: a graphical user interface for XAS analysis using IFEFFIT. Physica Scripta T T115, 1011–1014. https://doi.org/10.1238/Physica.Topical.115a01011.

Wieser, M.E., Buhl, D., Bouman, C., Schwieters, J., 2004. High precision calcium isotope ratio measurements using a magnetic sector multiple collector inductively coupled plasma mass spectrometer. J. Anal. At. Spectrom. 19, 844. https://doi.org/10.1039/b403339f.

Young, E.D., Galy, A., Nagahara, H., 2002. Kinetic and equilibrium mass-dependent isotope fractionation laws in nature and their geochemical and cosmochemical significance. Geochim. Cosmochim. Acta 66, 1095–1104. https://doi.org/10.1016/S0016-7037(01)00832-8.